Chemical vapor deposition of 3D graphene/carbon nanotubes networks for hybrid supercapacitors

Xining Zang[a], Yingqi Jiang[b], Mohan Sanghadasa[c], Liwei Lin[a],*

[a] Department of Mechanical Engineering, University of California, Berkeley, CA, 94704, USA
[b] Analog Devises Inc, Norwood, MA, 01887, USA
[c] U.S. Army Combat Capabilities Development Command Aviation & Missile Center, Redstone Arsenal, AL, 35898, USA

ARTICLE INFO

ABSTRACT

We present the direct synthesis of graphene as well as carbon nanotube within the vertically-aligned carbon nanotube (VACNT) forests to form either the 3D CNT-graphene or 3D CNT-CNT network by means of chemical vapor deposition (CVD). The multi-dimensional material assembly process is achieved by the electroplating of a thin nickel layer around the individual CNTs followed by a second CVD process for the synthesis of graphene or CNTs branching out of the original VACNT, respectively. The combinations of large surface areas (graphene and CNT), high electrochemical reactions sites (graphene), and metal particles as pseudocapacitor materials improve the electrochemical capacitance. Compared with as-grown CNT forests, the capacitance of 3D CNT/graphene networks increases 16 times to ~20 F/cm^3 and 3D CNT/CNT networks increase 25 times to ~30 F/cm^3. A flexible supercapacitor based on the CNT/CNT forest electrode is demonstrated to achieve 90 % retention of its original capacitance after 10,000 charging-discharging cycles.

1. Introduction

Highly conductive vertically-aligned carbon nanotube (VACNT) forests possessing enormous large surface areas can be further functionalized with various active materials [1,2] as platforms for many electrochemical applications, including catalysts, hydrogen evolution reactions, and energy storages [3,4]. For example, supercapacitors with both high power density and energy density [1,5,6] have been broadly studied as promising energy storage devices to replace batteries, including the usages of VACNT forests as the key platform [7–9]. Recent studies have demonstrated enhanced energy density of VACNT forests by the coating of pseudo-capacitance materials [10], such as conductive polymer [11], nickel particles [12], Manganese oxides [13] and Ruthenium dioxide [2,12,14]. In general, as grown VACNT forests are porous with more than 90 % of empty spaces [15]. The typical lateral conductivity of VACNT is low as the electron pathways in the lateral direction of the CNT network is less as compared to that of its longitude direction [16]. Branding and decorating the original CNT network with carbon materials including CNT and graphene [17,18] will greatly increase the electron pathway and further increase the surface related double layer capacitance [19].

Here, we demonstrate the feasibility of using a second chemical vapor deposition process after the growth of VACNT to construct CNT-graphene and CNT-CNT networks within the original VACNT forests. Nickel can serve as the catalyst in both the graphene and second CNT growth processes and it can also contribute as the pseudo-capacitance in hybrid supercapacitors. Such CNT-nickel-graphene and CNT-nickel-CNT networks greatly increase the surface areas and the cross-connections of VACNT forests for better electrical conductivity. Previously, several groups have demonstrated the assembly of CNT and graphene networks by: (1) physically mixing of graphene and CNT in solutions; (2) reducing graphene oxide to graphene in the mixture of CNT solutions [20,21]; and (3) growing CNT on multilayer graphene films by microwave plasma enhanced chemical vapor deposition technique and their field emission properties [22,23]. None of the above methods could enable the in-situ CNT/graphene grafting, while they could introduce damages to the electrode structures. Here, a second CVD process is conducted after the deposition of the nickel catalysts conformally and uniformly in the VACNT forests. Either graphene or CNT can be synthesized depending on the growth conditions and the resulting nanostructures show enhanced energy density for supercapacitors.

* Corresponding author.
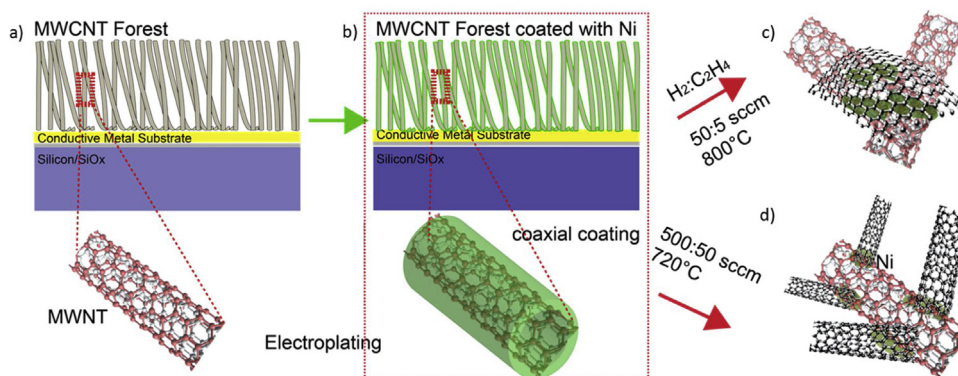E-mail address: lwlin@me.berkeley.edu (L. Lin).

Fig. 1. Schematic diagram showing the chemical vapor deposition process of the 3D graphene/CNT networks. (a) VACNT forest is grown on the Si/SiO$_2$ substrate with a metal conductive layer at the bottom using ion as the catalyst; (b) uniform coating of nickel onto individual CNTs by electroplating; (c) CVD of graphene on CNT/Ni at 800 °C with H$_2$:C$_2$H$_4$ flowing at 50:5 sccm. Nickel droplets are formed due to the high temperature process and aggregated together; (d) CVD of second CNT structures with nickel particles as the catalysts within the VACNT forest at 720 °C with H$_2$:C$_2$H$_4$ flowing at 500:50 sccm.

The two-step CVD process is illustrated in Fig. 1: a) multiwall carbon nanotube (MWCNT) forests are synthesized by chemical vapor deposition; b) nickel is coaxially coated onto CNTs by electroplating, and a second CVD process is executed to grow CNT or graphene within the VACNT forests. It is found that temperature and gas flow in the second CVD process greatly affects the growth results to be discussed later. The application of graphene/CNT networks as electrodes for supercapacitors, including a flexible supercapacitor package with a solid-state electrolyte, have been successfully demonstrated. Experimental results show a prototype supercapacitor can preserve its energy storage performance under mechanical bending of 90 degrees to retain >90 % of its storage capacity after 10,000 charging-discharging cycles. As such, the 3D graphene/CNT networks presented in this work could be extended to energy storage and many other applications in the field of electrochemical reactions, such as electrodes for sensors and energy storage devices.

2. Experimental

2.1. Synthesis of vertical aligned CNT forest

Multiwall carbon nanotube in the form of VACNT forest is synthesized on the Si/SiO$_2$ substrate with e-beam depositions of Mo/Al/Fe (50 nm/10 nm/5 nm) as the conducting/catalyst bottom layer. E-beam deposition is performed in order of Mo-Al-Fe, with a deposition rate of 1 A/min. In the CVD process, a quartz tube furnace is programmed to ramp up to 720 °C within 30 min with 40 sccm of H$_2$ flowing continuously. The furnace is then maintained at 720 °C for 20 min. with H$_2$:C$_2$H$_4$ flowing at 611:90 sccm. After the process, the quartz tube is pulled out and cooled down in the open air.

2.2. Coating of the nickel layer onto CNT forest by electroplating

Nickel is conformally deposited onto VACNT using electrochemical plating. NiSO$_4$ with cyanide as the stabilizer is used as the aqueous electrolyte. Before electroplating, a vacuum is first performed to remove air and force electrolyte (to be added later) to penetrate the VACNT forest. A direct DC current density of 10 mA/cm^2 is used with the VACNT forest as the cathode. VACNT coated with nickel is dried in air for 24 h without heating or vacuum to maintain the vertically aligned structure.

2.3. Second chemical vapor deposition to grow graphene/CNT

A second CVD is performed with two gases, H$_2$ and C$_2$H$_4$. In the CVD process, a quartz tube furnace is programmed to ramp up to with a rate of 20 °C/min with 40 sccm of H$_2$ flowing continuously. Ethylene is added when the temperature reaches the set reaction temperature. The flow rate of H$_2$:C$_2$H$_4$ is tuned to the reaction recipe - 500:50 sccm for graphene and 50:5 sccm for CNT, respectively. The reaction time is set for 10 min., setting temperature at 720 °C, 760 °C, and 800 °C. After the CVD process, all gases are turned off and the furnace is cooled down to ambient temperature.

2.4. Imaging and other characterizations of the materials

SEM images and TEM images are taken by LEO 1550 and Tecnai 12 TEM. Cross-sectional SEM samples are prepared by breaking the samples after putting them in liquid nitrogen for 30 s. TEM samples are prepared by scratching the material from the substrate and dispersing them in ethanol and dropped onto TEM copper grid (Quantifoil). Raman spectrum is obtained using Renishaw InVia, with 633 nm laser.

2.5. Electrochemistry tests

Electrochemical tests of the fabricated electrodes are performed by an electrochemical workstation (Gamry 600, PHE 200). Capacitance is tested using the Cyclic Voltammetry mode and 1 Mol/L KOH aqueous solution is used as the electrolyte. The three-electrode cell configuration is set up using potassium as the counter electrode, fabricated 3D nanostructure electrode as the working electrode, and Ag/AgCl as the reference electrode. The working electrode is constructed as 1 cm × 0.5 cm in size for evaluations. Various scanning rates of 10, 20, 50, and 100 mV/s are tested.

2.6. Flexible CNT/CNT supercapacitor assembly and testing

The CNT + Ni + CNT film is peeled off using the Kapton tape and cut into 1 cm × 1 cm pieces. It is first dipped into pure H$_3$PO$_4$ for 120 s to activate the surface for better wettability. The electrolyte is made of the H$_3$PO$_4$/PVA/H$_2$O mixture with a mass ratio of 1:1:8 under continuously stirring for 1 h at 80 °C. About 100 μl of the electrolyte is applied to the individual electrode and dried for 15 min. When the electrolyte is almost dried, two electrodes are pressed and dried together to complete the assembly process and the electrolyte in between the two electrodes is also utilized as a separator.
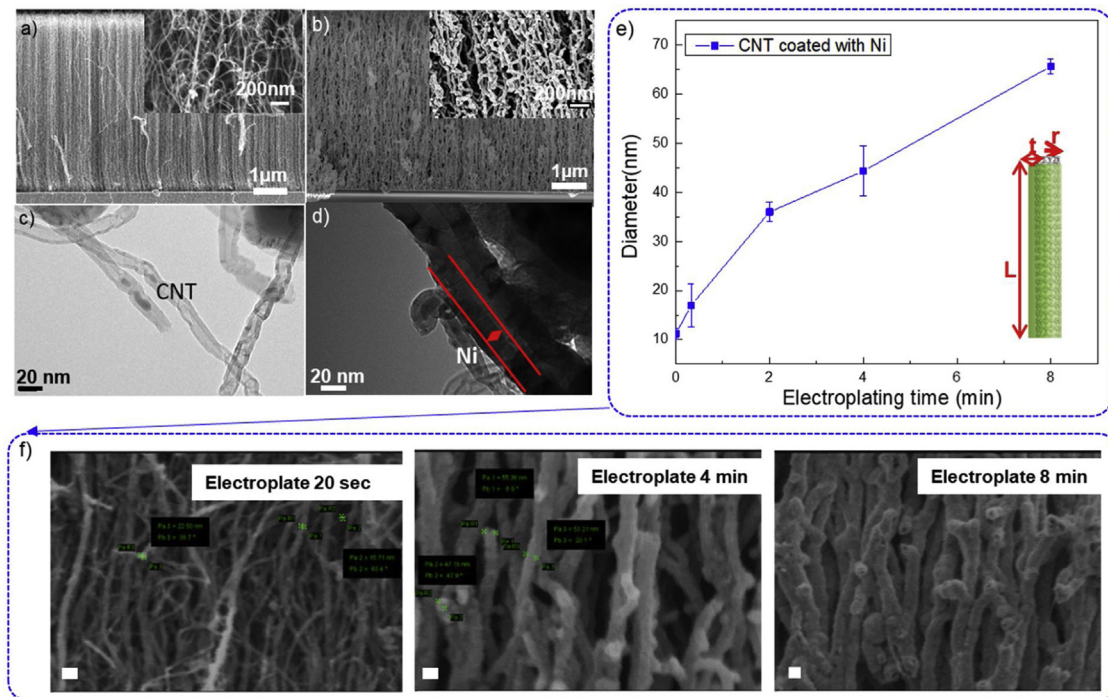
Fig. 2. (a) vertical aligned carbon nanotube (VACNT), inset: close-up view of VACNT. (b) After coating of a 30 nm-thick nickel on individual CNTs by the electroplating process. (c) and (d) TEM images for (a) and (b), respectively. (e) The diameter of the CNT coated with electroplated nickel layer vs the electroplating time. (f) SEM of CNT electroplated with nickel for a different time. The numbers on Fig. 2f are presented in Fig. 2e.

The packaged supercapacitor is tested at different bending angles (30°, 60°, and 90°) with a scanning rate of 200 mV/s. A packaged symmetric supercapacitor is tested for 10,000 cyclic voltammetry cycles at the 2 V/s scan rate.

3. Results and discussion

In the first CVD process, 20 μm long vertical aligned CNT forest is grown using a well-developed recipe [24] (Fig. 2a). The as-grown CNT has the diameter of around 20 nm (Fig. 2b). TEM images imply that the CNTs should be multiwall as the wall thickness is around 2−5 nm [25]. Fig. 2c and d show ∼15 nm-thick nickel film is coated coaxially onto the individual CNT after 2 min. of the electroplating process. The diameter of coated CNT increases linearly with respect to the electroplating time as plotted in Fig. 2e in the first 8 min. of the electroplating process with a slope of a roughly 7.5 nm/min rate. SEM and TEM images both prove the uniformity of the nickel coating process (Fig. 2f). As-grown CNTs are vertically aligned in as shown in Fig. 2a and the CNTs are connected with each other by physically twisting and knitting as can be seen in the inset of Fig. 2a to form electrical pathways. The nickel electroplating process can uniformly deposit a thin nickel layer around the CNTs (Fig. 2b) to increase the conductivity of VACNT forest as the measured sheet resistance decreases from the original VACNT at ∼100 Ω/□ to nickel-coated VACNT at ∼80 Ω/□.

In the second CVD process, both graphene and CNT have been synthesized onto the VACNT forest depending on the process temperature and gas flow conditions. For the graphene flakes (Figures 3a&b), the process temperature is 800 °C with $H_2:C_2H_4$ flowing at 50:5 sccm using the nickel particles as the catalysts. The thin nickel film can melt and deform during the high temperature process due to the melting temperature depression effect for nanostructures. Melting temperature decreases with the critical size of nanostructure, which is the thickness of nickel film. The characterizations of synthesized graphene sheet are validated by Raman Spectrum analysis as shown in Figure 3c. The decreases of I_D and increases

of I_G and I_{2D} peaks after the graphene synthesis process imply the graphene formation. Furthermore, the ratio of I_G / I_{2D} is about 0.5 ∼1.0 and this could suggest that the as-grown graphene flake has the structure of double layer [26]. Graphene flakes can connect laterally with the carbon nanotubes to increase the surface areas and electron pathways. As shown in Fig. 4, the sheet resistance of graphene flakes decorated CNT forest is further decreased to 70 Ω/□ from the nickel coated VACNT at 80 Ω/□.

For the synthesis of the second coating of CNTs onto the VACNT forest, the process temperature is set at 700 °C with $H_2:C_2H_4$ flowing at 500:50 sccm using the nickel particles as the catalysts. Fig. 3d and e show the SEM images of the synthesis results with more CNT "branches" growing out of the VACNT forest. Diameters of newly-grown CNTs vary widely from 10 nm to 100 nm due to the non-uniform aggregations of nickel particles. In the first CVD process to grow vertical aligned carbon nanotube, the thin catalyst layer dewet uniformly and induce uniform distribution of CNT diameter. Meanwhile during the second the CVD process, the electroplated nickel will deform to non-uniform structures. As such the synthesized CNT has wide distribution of diameter. After the process, the sheet resistance is further reduced to 50 Ω/sq. The Raman Spectrum analyses in Fig. 3f show no obvious changes in the 2D peak and the G/2D ratio, implying similar characteristics of multiwall CNTs before and after the synthesis process. The slightly split of the G peak in Fig. 3f is probably due to the defective graphite-like structure in the thick wall CNTs [27]. The G' peak split from G peak corresponds to the transverse wave (TO) mode perpendicular to the axis. The frequency of G peak appears near 1600 cm^{-1} regardless of the diameter of the carbon nanotube, while the frequency of the G-peak changes in inverse proportion to the square of the diameter.

The growth processes of Graphene and CNT strongly depend on the synthesis parameters such as temperature and gas flow rates with experimental details summarized in Table 1. It is observed that high partial pressure of C_2H_4 and H_2 is in favor of the growth of CNTs [28,29]. On the other hand, high temperature is in favor of the growth of graphene due to more effective pyrolysis process
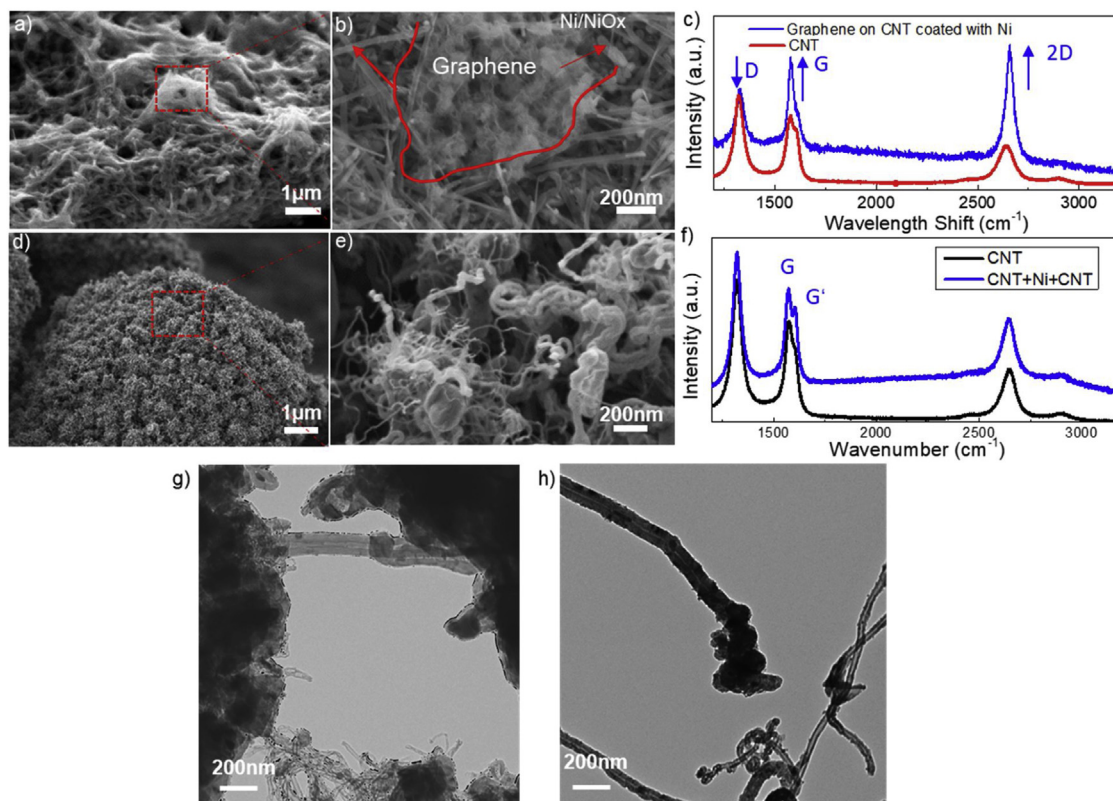
Fig. 3. CVD graphene synthesized on nickel-coated VACNT forest: (a) SEM image; (b) enlarge view of (a) showing a possible graphene sheet wrapping Ni/NiOx nanoparticles as highlighted in the red boundary; (c) Raman spectrum showing decrease in the D peak and increase in 2D peak with the low ratio of I_G/I_{2D} as the evidence of graphene. Second CVD CNT synthesized on nickel-coated VACNT forest (d) SEM image of CNTs growing on the VACNT forest; (e) close-up view SEM image; (f) Raman spectrum showing similar characteristics before and after the second CVD CNT growth process; (g) (h) Transmission electron microscopy (TEM) image of (e). (For interpretation of the references to colour in this figure legend, the reader is referred to the web version of this article).

Table 1
Summary of the second CVD process, and the sheet resistance changes.

TemPERature ^{o}C	Flow Rate (sccm)C_2H_4:H_2	CVD Product
800	5:50	graphene
760	5:50	graphene
720	5:50	Amorphous Carbon
800	50:500	CNT
760	50:500	CNT
720	50:500	CNT

Fig. 4. Sheet resistance of CNT, CNT-Ni, CNT-graphene, and CNT-CNT.

[30]. Both the syntheses of graphene and CNT are based on the carbon absorption and segregation process [31]. The pressure is remained at atmosphere pressure, while high partial gas pressure is in favor of the synthesis of CNTs as more carbon atoms are available in the process. As such CNT is branched onto the original CNT structure using 50:500 sccm of C_2H_4:H_2 [32,33]. Furthermore, if the temperature is set at 720 °C with low gas pressure (H_2:C_2H_4 = 50:5 sccm), amorphous carbon is the product due to the incomplete pyrolysis of ethylene as previously reported [34]. In other CVD technique such as Microwave Plasma-enhanced Chemical Vapor Deposition (MWCVD), the synthesized carbon nanostructure also highly depends on the plasma parameters beside temperature and gas which is simplified in a ambient pressure CVD as presented in this paper [32].

For practical application, the synthesized CNT/Ni/Graphene and CNT/Ni/CNT networks are tested as the supercapacitor electrodes in Fig. 5a and b. In both cases, nickel can be oxidized in the process to nickel oxide and to work as the pseudo-capacitance material with the charge transfer from Ni^{2+} to Ni^{3+} as demonstrated previously [12]. R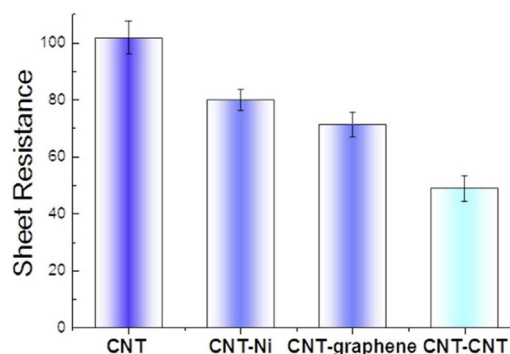esults show that both newly synthesized networks of CNT/Ni/Graphene and CNT/Ni/CNT structure have a specific capacitance of 25.1 m F/cm^2 and 34.2 m F/cm^2 or about 2.24 and 3.19 times higher capacitance, respectively, as compared with electrodes made of CNT/Ni forests. When compared with original CNT forests (1.56 m F/cm^2), the CNT/Ni/Graphene and CNT/Ni/CNT networks show 16.1 and 25.5 times higher capacitance, respectively. Considering the averaged VACNT thickness is ~10.8 μm, the volumetric capacitance of CNT/Ni/Graphene and CNT/Ni/CNT supercapacitors are ~20 F/cm^3 and ~30 F/cm^3, respectively. The CNT/Ni/CNT network shows better synchronization of current as the current increase in the CNT/Ni/Graphene network is only obvious near the 0.2 V mark probably due to the redox peak of nickel-nickel. It is believed that the CNT/Ni/CNT network has larger surface area than the CNT/Ni/Graphene network to result in higher double layer capacitance while the latter network has
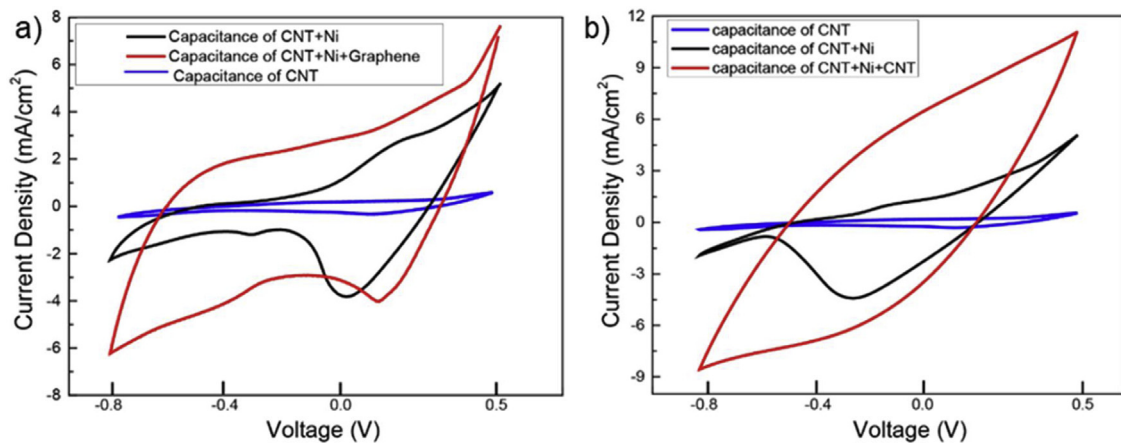
Fig. 5. (a) Cyclic voltammetry characterizations of CNT (blue), CNT/nickel (black), and CNT/Ni/Graphene network (red). (b) Cyclic voltammetry characterizations of CNT (blue), CNT/nickel (black) and CNT/Ni/CNT network (red). (For interpretation of the references to colour in this figure legend, the reader is referred to the web version of this article).

stronger nickel–nickel pseudocapacitance. The second CVD process significantly promotes the surface related double layer capacitance over the Ni/NiO_x pseudocapacitance. The asymmetry redox peak around 0.2 V is not shown in the cyclic voltammetry test since the scan range is not negative enough for water splitting [35].

Results from the electrochemical tests reveal that the CNT/Ni/CNT network has the better performance. As such, a flexible supercapacitor [36] package has been constructed based on the CNT/Ni/CNT networks. The Kapton tape is used to peel off the CNT/Ni/CNT forest (top in Fig. 6a), a 25 μm-thick stainless steel

mechanical supporter is glued at the back side (middle figure in Fig. 5a). An electrolyte made of 1:1:8 H_3PO_4/PVA/H_2O is selected as both the solid-state electrolyte and separator [37]. Packaged supercapacitors are tested under different bending angles from 30 to 90 degrees, as shown in Fig. 6b. Results in Fig. 6c shows the coherent cyclic voltammetry results under different bending angles with little changes. Using a scanning rate of 200 mV/s, the flexible supercapacitor shows a projection capacitance of ∼10 m F/cm^2. The low ion mobility in the solid-state electrolyte and high electrolyte-electrode resistance result in low specific capacitance.
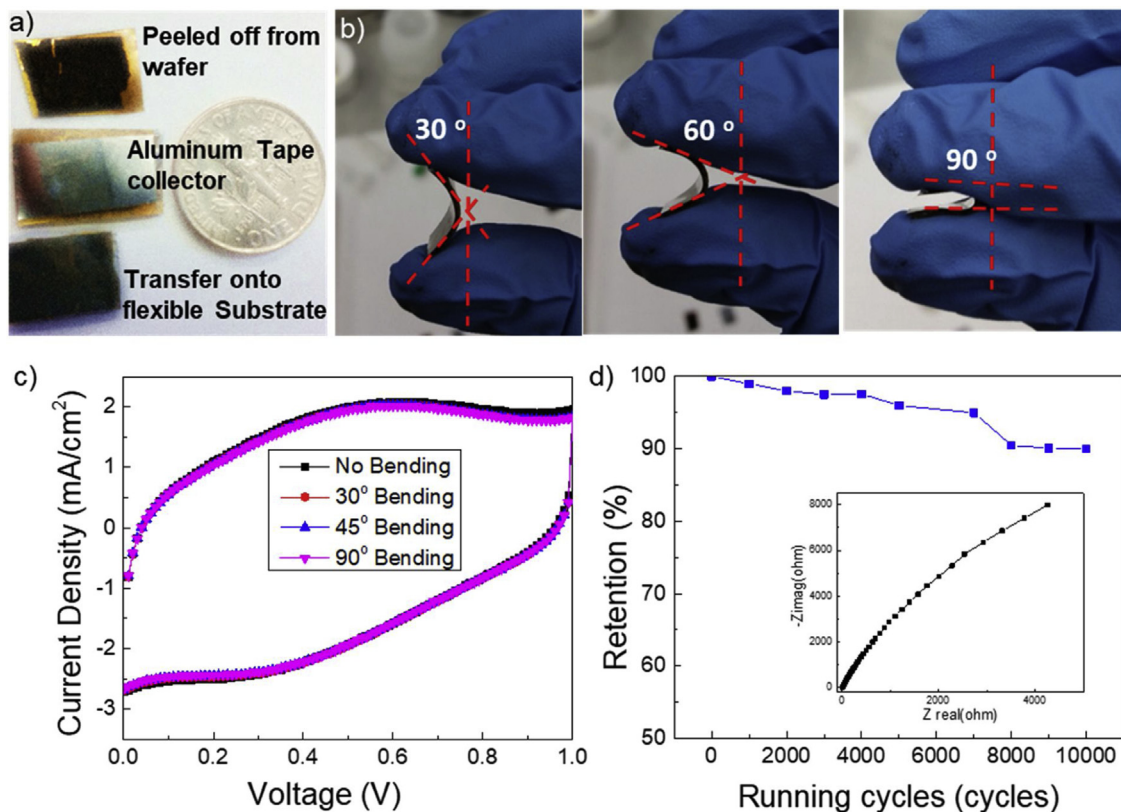

Fig. 6. (a) and (b)Packaging of flexible supercapacitor based on two CNT/Ni/CNT electrodes and H_3PO_4/PVA solid-state electrolyte. The Kapton tape is used to peel off the CNT/Ni/CNT film from the SOI wafer, and a stainless steel is taped at the back side as both charge collector and mechanical supporter. (c) Cyclic Voltammetry of flexible supercapacitor under different angles, with a scanning rate of 200 mV/s. (d) 10,000 cycles CV test of the same supercapacitor in (c), using a scanning rate of 2 V/s. Inset: impedance measurement of the CNT/Ni/CNT electrode.

The prototype package also causes the low specific volume capacitance which can be improved by thinning the packaging substrate. The cyclic CV tests in Fig. 6d for over 10,000 cycles show good stability with an over 90 % retention. Also shown in the inset of Fig. 6d is the impedance measurement of the CNT/Ni/CNT electrode with low AC resistance.

4. Conclusions

In this paper, we first design and demonstrate a two-step CVD process to fabricate CNT-graphene and CNT-CNT 3D matrix electrodes which are used in supercapacitors. The second CVD process directly synthesizes graphene and CNT onto the pre-grown VACNT forests, which not only increase the active surface area but also improve the electrical conductivity. The capacitance of CNT/Ni/CNT network increases 16 times and the capacitance of the CNT/Ni/Graphene network increases 25 times as compared with that of as-grown VACNT (without nickel coating). Such hybrid CNT/Ni/CNT and CNT/Ni/Graphene networks not only modify the electrical conductivity but also have increased surface areas for potential versatile applications.

Author statement

X.Zang and L. Lin designed the research; X. Zang performed the experiment and wrote the paper; Y. Jiang provided guidance on the experiment; M. Sanghadasa provide discussion and comments on the paper.

Declaration of Competing Interest

The authors declare that they have no known competing financial interests or personal relationships that could have appeared to influence the work reported in this paper.

Acknowledgment

References

[1] A.G. Pandolfo, A.F. Hollenkamp, Carbon properties and their role in supercapacitors, J. Power Sources 157 (1) (2006) 11–27.

[2] R. Warren, F. Sammoura, K.S. Teh, A. Kozinda, X.N. Zang, L.W. Lin, Electrochemically synthesized and vertically aligned carbon nanotube-polypyrrole nanolayers for high energy storage devices, Sens. Actuators A-Phys. 231 (2015) 65–73.

[3] T. Chen, L.M. Dai, Carbon nanomaterials for high-performance supercapacitors, Mater. Today 16 (7–8) (2013) 272–280.

[4] R.H. Baughman, A.A. Zakhidov, W.A. de Heer, Carbon nanotubes - the route toward applications, Science 297 (5582) (2002) 787–792.

[5] X. Zang, C.W. Shen, Y. Chu, B.X. Li, M.S. Wei, J.W. Zhong, M. Sanghadasa, L.W. Lin, Laser-induced molybdenum carbide-graphene composites for 3D foldable paper electronics, Adv. Mater. 30 (26) (2018), 1800062.

[6] X. Zang, Q. Zhou, J.Y. Chang, Y.M. Liu, L.W. Lin, Graphene and carbon nanotube (CNT) in MEMS/NEMS applications, Microelectron. Eng. 132 (2015) 192–206.

[7] K. Hata, D.N. Futaba, K. Mizuno, T. Namai, M. Yumura, S. Iijima, Water-assisted highly efficient synthesis of impurity-free single-waited carbon nanotubes, Science 306 (5700) (2004) 1362–1364.

[8] X. Zang, C. Shen, E. Kao, R. Warren, R. Zhang, K.S. Teh, J. Zhong, M. Wei, B. Li, Y. Chu, M. Sanghadasa, A. Schwartzberg, L. Lin, Titanium disulfide coated carbon nanotube hybrid electrodes enable high energy density symmetric pseudocapacitors, Adv. Mater. 30 (5) (2018), 1704754.

[9] X.N. Zang, C.W. Shen, M. Sanghadasa, L.W. Lin, High-voltage supercapacitors based on aqueous electrolytes, Chemelectrochem 6 (4) (2019) 976–988.

[10] Z. Zheye, X. Fei, Q. Lihua, X. Junwu, W. Shuai, L. Yunqi, Facile synthesis of 3D MnO2–graphene and carbon nanotube–graphene composite networks for high-performance, flexible, all-solid-state asymmetric supercapacitors, Adv. Energy Mater. 4 (10) (2014), 1400064.

[11] Z.Y. Zhang, K. Chi, F. Xiao, S. Wang, Advanced solid-state asymmetric supercapacitors based on 3D graphene/MnO2 and graphene/polypyrrole hybrid architectures, J. Mater. Chem. A 3 (24) (2015) 12828–12835.

[12] Y.Q. Jiang, P.B. Wang, X.N. Zang, Y. Yang, A. Kozinda, L.W. Lin, Uniformly embedded metal oxide nanoparticles in vertically aligned carbon nanotube forests as pseudocapacitor electrodes for enhanced energy storage, Nano Lett. 13 (8) (2013) 3524–3530.

[13] Z.Y. Zhang, F. Xiao, S. Wang, Hierarchically structured MnO2/graphene/carbon fiber and porous graphene hydrogel wrapped copper wire for fiber-based flexible all-solid-state asymmetric supercapacitors, J. Mater. Chem. A 3 (21) (2015) 11215–11223.

[14] X.N. Zang, Q. Zhou, J.Y. Chang, Y.M. Liu, L.W. Lin, Graphene and carbon nanotube (CNT) in MEMS/NEMS applications, Microelectron. Eng. 132 (2015) 192–206.

[15] O. Yaglioglu, A.Y. Cao, A.J. Hart, R. Martens, A.H. Slocum, Wide range control of microstructure and mechanical properties of carbon nanotube forests: a comparison between fixed and floating catalyst CVD techniques, Adv. Funct. Mater. 22 (23) (2012) 5028–5037.

[16] T.W. Ebbesen, H.J. Lezec, H. Hiura, J.W. Bennett, H.F. Ghaemi, T. Thio, Electrical conductivity of individual carbon nanotubes, Nature 382 (6586) (1996) 54–56.

[17] W. Wang, S.R. Guo, K.N. Bozhilov, D. Yan, M. Ozkan, C.S. Ozkan, Intertwined nanocarbon and manganese oxide hybrid foam for high-energy supercapacitors, Small 9 (21) (2013) 3714–3721.

[18] O.S. Panwar, A.K. Kesarwani, S.R. Dhakate, B.S. Satyanarayana, Graphene synthesized using filtered cathodic vacuum arc technique and its applications, Vacuum 153 (2018) 262–266.

[19] K.H. An, W.S. Kim, Y.S. Park, J.M. Moon, D.J. Bae, S.C. Lim, Y.S. Lee, Y.H. Lee, Electrochemical properties of high-power supercapacitors using single-walled carbon nanotube electrodes, Adv. Funct. Mater. 11 (5) (2001) 387–392.

[20] Z. Yan, L.L. Ma, Y. Zhu, I. Lahiri, M.G. Hahm, Z. Liu, S.B. Yang, C.S. Xiang, W. Lu, Z.W. Peng, Z.Z. Sun, C. Kittrell, J. Lou, W.B. Choi, P.M. Ajayan, J.M. Tour, Three-dimensional metal-graphene-nanotube multifunctional hybrid materials, ACS Nano 7 (1) (2013) 58–64.

[21] H.Y. Sun, Z. Xu, C. Gao, Multifunctional, ultra-flyweight, synergistically assembled carbon aerogels, Adv. Mater. 25 (18) (2013) 2554–2560.

[22] A. Bisht, S. Chockalingam, O.S. Panwar, A.K. Kesarwani, B.P. Singh, V.N. Singh, Growth of dense CNT on the multilayer graphene film by the microwave plasma enhanced chemical vapor deposition technique and their field emission properties, RSC Adv. 5 (109) (2015) 90111–90120.

[23] A.K. Kesarwani, O.S. Panwar, S. Chockalingam, A. Bisht, S.R. Dhakate, B.P. Singh, A.K. Srivastava, R.K. Rakshit, Graphene synthesized from solid carbon source using filtered cathodic vacuum arc technique for transparent conducting and field effect transistor devices, Sci. Adv. Mater. 6 (10) (2014) 2124–2133.

[24] Y.Q. Jiang, P.B. Wang, L.W. Lin, Characterizations of contact and sheet resistances of vertically aligned carbon nanotube forests with intrinsic bottom contacts, Nanotechnology 22 (36) (2011).

[25] J. Cumings, A. Zettl, Low-friction nanoscale linear bearing realized from multiwall carbon nanotubes, Science 289 (5479) (2000) 602–604.

[26] X.N. Zang, L.W. Lin, Graphene synthesis via droplet cvd and its photonic applications, 2014 IEEE 27th International Conference on Micro Electro Mechanical Systems (Mems) (2014) 486–489.

[27] J.H. Lehman, M. Terrones, E. Mansfield, K.E. Hurst, V. Meunier, Evaluating the characteristics of multiwall carbon nanotubes, Carbon 49 (8) (2011) 2581–2602.

[28] A. Bisht, S. Chockalingam, O.S. Panwar, A.K. Kesarwani, B.P. Singh, V.N. Singh, Substrate bias induced synthesis of flowered-like bunched carbon nanotube directly on bulk nickel, Mater. Res. Bull. 74 (2016) 156–163.

[29] A. Bisht, S. Chockalingam, O.S. Panwar, A.K. Kesarwani, I. Rawal, B.P. Singh, V.N. Singh, Structural, field emission and ammonia gas sensing properties of multiwalled carbon nanotube-graphene like hybrid films deposited by microwave plasma enhanced chemical vapor deposition technique, Sci. Adv. Mater. 7 (7) (2015) 1424–1434.

[30] X. Zang, Q. Zhou, J.Y. Chang, K.S. Teh, M.S. Wei, A. Zettl, L.W. Lin, Synthesis of single-layer graphene on nickel using a droplet CVD process, Adv. Mater. Interfaces 4 (4) (2017), 1600783.

[31] Y.H. Yun, V. Shanov, Y. Tu, S. Subramaniam, M.J. Schulz, Growth mechanism of long aligned multiwall carbon nanotube arrays by water-assisted chemical vapor deposition, J. Phys. Chem. B 110 (47) (2006) 23920–23925.

[32] A. Bisht, S. Chockalingam, O.S. Panwar, A.K. Srivastava, A.K. Kesarwani, Synthesis of nanostructure carbon films deposited by microwave plasma-enhanced chemical vapor deposition technique at room temperature, Fuller. Nanotubes Car. N. 23 (5) (2015) 455–462.

[33] A.K. Kesarwani, O.S. Panwar, S.R. Dhakate, R.K. Rakshit, V.N. Singh, A. Bisht, A. Kumar, Growth of single and bilayer graphene by filtered cathodic vacuum arc technique, J. Vac. Sci. Technol. A 34 (2) (2016).

[34] D.N. Futaba, J. Goto, S. Yasuda, T. Yamada, M. Yumura, K. Hata, General rules governing the highly efficient growth of carbon nanotubes, Adv. Mater. 21 (47) (2009), 4811-+.

[35] O. Khaselev, J.A. Turner, A monolithic photovoltaic-photoelectrochemical device for hydrogen production via water splitting, Science 280 (5362) (1998) 425–427.

[36] Z.Y. Zhang, F. Xiao, J. Xiao, S. Wang, Functionalized carbonaceous fibers for high performance flexible all-solid-state asymmetric supercapacitors, J. Mater. Chem. A 3 (22) (2015) 11817–11823.

[37] C. Zhao, C.Y. Wang, Z.L. Yue, K.W. Shu, G.G. Wallace, Intrinsically stretchable supercapacitors composed of polypyrrole electrodes and highly stretchable gel electrolyte, ACS Appl. Mater. Interfaces 5 (18) (2013) 9008–9014.

Biographies

Dr. Xining Zang was a PhD student under the supervision of Prof. Liwei Lin in Mechanical Engineering at University of California, Berkeley. Her PhD research focused on synthesis and assembly of low dimensional materials and their applications in sensing and energy storage. She currently works at MIT as a postdoc associate.

Dr. Yingqi Jiang was a PhD student under the supervision of Prof. Liwei Lin in Mechanical Engineering at University of California, Berkeley. His PhD research focused on carbon nanotube-based energy storage, particularly MEMS supercapacitor. Before his PhD, he got bachelor and master degrees with major of Electronic Science and Technology in Tsinghua University, China. He currently works at Analog Devices Inc. for MEMS R&D research.

Dr. Mohan Sanghadasa was a Faculty of University of Alabama, Huntsville (UAH), for 12 years. He is currently a Senior Research Scientist with the AMRDEC, U.S. Army. He also leads research programs on the development of nanotechnology enhanced sensors and energy storage systems. During his academic career, he has also conducted research on optical limiting, optical switching, and optical pattern recognition. His research activities with UAH were primarily in the area of nonlinear optics. His research activities with AMRDEC were on the development of micro devices, and polymer based modulators for IFOGs in inertial measurement units.

Prof Liwei Lin received the Ph.D. degree in mechanical engineering from the University of California at Berkeley (UC-Berkeley) in 1993. He joined UC-Berkeley in 1999, where he is currently a Professor with the Mechanical Engineering Department and a Co–Director with the Berkeley Sensor and Actuator Center. He has 20 issued U.S. patents in the area of MEMS/NEMS. His research interests are in design, modeling and fabrication of micro/nano structures, micro/nano sensors and micro/nano actuators, mechanical issues in micro/nano systems including heat transfer, and solid/fluid mechanics and dynamics. He is an ASME Fellow. He was a recipient of the 1998 NSF CAREER Award for research in MEMS packaging and the 1999 ASME Journal of Heat Transfer Best Paper Award for his work on micro scale bubble formation. He led the effort to establish the MEMS Division in ASME and served as the Founding Chairman of the Executive Committee from 2004 to 2005. He was the general Co–Chair of the IEEE 24th international conference on Micro Electro Mechanical Systems in 2011.